Int. J. Environ. Sci. Technol. (2015) 12:183–192
DOI 10.1007/s13762-013-0438-2

ORIGINAL PAPER

Maxwell–Stefan based modelling of ion exchange systems containing common species (Cd^{2+}, Na^{+}) and distinct sorbents (ETS-4, ETS-10)

P. F. Lito · J. P. S. Aniceto · C. M. Silva

Received: 4 January 2012 / Revised: 21 October 2013 / Accepted: 12 November 2013 / Published online: 19 December 2013

Abstract Cadmium(II) is a toxic hazardous cation, whose presence in the environment causes great concern because of its bioaccumulation in organisms and bioamplification along food chain. Hence, the removal of cadmium compounds from industrial waters and wastewaters is particularly essential, which requires intensive experimental and modelling studies to deal with the problem. In this work, the ion exchange of Cd^{2+} ions from aqueous solution using microporous titanosilicates (ETS-4 and ETS-10) has been modelled using adapted Maxwell–Stefan equations for the ions transport inside the sorbent particles. The fundamentals of the Maxwell–Stefan equations along with correlations for the convective mass transfer coefficients have been used with advantage to reduce the number of model parameters. In the whole, the model was able to represent successfully the kinetic behaviour of 11 independent and very distinct curves of both studied systems (Cd^{2+}/Na^{+}/ETS-4 and Cd^{2+}/Na^{+}/ETS-10). The predictive capability of the model has been also shown, since several uptake curves were accurately predicted with parameters fitted previously to different sets of experimental data.

Keywords Cadmium(II) · ETS-4 · ETS-10 · Ion exchange · Maxwell–Stefan · Modelling

Introduction

The presence of toxic metals in the environment has an adverse impact on the living organisms and aquatic systems given their toxicology and bioaccumulation tendency. Their massive application in many industrial processes, mainly metal finishing, welding, alloy manufacturing plants, pulp industries and petroleum refining, inevitably results in their discharge back into the environment (Siegel 2002). As a result, industries have been forced to reduce metal contents in their wastewaters and effluents to acceptable levels (Dabrowski et al. 2004).

Cadmium is one of the most toxic substances whose presence and accumulation in soil and plants can cause serious damage to the human health and the ecosystems (Otero et al. 2009). Its well-known harmful effects on human health have prompted its classification by the European Union as “priority hazardous substance” (Decision No. 2455/2001/EC), and accordingly cadmium must be eliminated from discharges and emissions within an appropriate timetable that shall not exceed twenty years.

Cadmium occurs naturally on the earth’s crust, mainly associated with zinc and non-ferrous ores, being commercially obtained as a by-product of zinc smelting (Clark et al. 2001). It has found wide applications, for instance, as stabilizers and pigments in plastics, in electroplating, in solders and other alloys, as well as in fossil fuels (Clark et al. 2001; Økland et al. 2005), and in Ni–Cd batteries. As a result, cadmium is released into the environment by industrial wastewaters as well as through fertilizers. In addition, impurities in the zinc of galvanized pipes and solders and some metal fittings may also contribute to drinking water contamination with cadmium.

The persistence of cadmium in the aquatic systems encourages the development of effective techniques to

P. F. Lito · J. P. S. Aniceto · C. M. Silva (✉)
CICECO/Department of Chemistry, University of Aveiro,
Campus Universitário de Santiago, 3810-193 Aveiro, Portugal
e-mail: carlos.manuel@ua.pt

reduce cadmium concentration in water and industrial waters. Ion exchange has been considered one of the most attractive technologies to remove toxic metals from aqueous solutions (Dabrowski et al. 2004). Besides its simple and efficient application, ion exchange is effective to remove even trace concentrations of pollutants from aqueous solutions, being extremely appropriate for tertiary treatments of wastewaters.

Titanosilicates are an important class of zeolite-type materials which have attracted increasing attention because of their high stability, ion exchange properties, and remarkable selectivity. These materials have a well-defined crystalline structure formed by a three-dimensional combination of tetrahedral and octahedral building blocks carrying a −2 global charge neutralized by extra-framework exchangeable cations which confer them a high cation exchange capacity (Lv et al. 2007).

Recent studies have demonstrated the high capacity of titanosilicate materials toward toxic metals. For instance, ETS-10 has been shown to have high selectivity for several toxic metals such as Pb^{2+}, Cu^{2+}, Cd^{2+}, Co^{2+}, Mn^{2+}, Zn^{2+} (Choi et al. 2006; Lv et al. 2007; Camarinha et al. 2009). Lopes et al. (2007, 2009) evaluated the potential of synthetic microporous (ETS-4, ETS-10, and AM-2) and layered (AM-4) titanosilicates for decontamination of natural waters polluted with low mercury levels and found they have a great potential for wastewater purification. Barreira et al. (2009) and Ferreira et al. (2009) investigated the capacity of ETS-4 to uptake cadmium(II). Both studies reveal the large ion exchange capacity of ETS-4 and their high removal efficiencies. Accordingly, the possibility of synthesizing pellets of supported titanosilicates is welcome in view of the fact they are absolutely necessary for practical and commercial wastewater and water treatment. Until now, only microparticle crystals have been studied.

Modelling and simulation are fundamental tools in the prediction of the dynamic behaviour, optimization of operating conditions, and scaling up of chemical plants. This work focuses the modelling of ion exchange kinetics since its accurate representation is crucial for computer-aided design of several applications, as for instance, softening and deionization of water, waste treatment, catalysis, chemicals purification, plating, food and pharmaceutical uses.

In electrolyte solutions, the electrical field induced by the different mobility of counter ions produces an additional force responsible for the transport of ions. The Nernst–Planck (NP) equations can be effectively applied to describe mass transport in ionic systems, accounting for both concentration and electric potential gradients (Smith and Dranoff 1964; Chanda and Rempel 1995; Dolgonosov et al. 1995; Patzay 1995; Rodriguez et al. 1998, 2002; Samson and Marchand 1999; Varshney and Pandith 1999; Varshney et al. 2003; Valverde et al. 2004; Cincotti et al. 2006). Nonetheless, NP model does not take non-ideality effects into account, which limits its applicability to dilute ionic systems (Helfferich 1995; Wesselingh et al. 1995). In addition, the NP interdiffusion coefficients of counter ions are composition-dependent and the ionic interactions (ion–ion, ion–solvent, and ion–ion exchanger) are lumped into effective diffusivities (Helfferich 1995). On the other hand, Maxwell–Stefan (MS) equations may be considered a more reliable approach to describe ion exchange (Graham and Dranoff 1982a, b; Pinto and Graham 1987; Wesselingh et al. 1995; Krishna and Wesselingh 1997). Beyond their extensive application in non-ionic systems, the MS model has recently found relevance for electrolyte mixtures, mainly in membrane electrolysis (e.g. van der Stegen et al. 1999; Hogendoorn et al. 2001) and electrodialysis (Kraaijeveld et al. 1995). In contrast to the NP model, the MS equations do take into account and distinguish both ion–ion and ion–solid interactions and define one diffusivity coefficient for each pair of components, being dependent on their properties only and softly composition-dependent (Silva and Lito 2007; Lito and Silva 2008; Lito et al. 2013).

In this work, the simultaneous modelling of two independent ion exchange systems, namely Cd^{2+}/Na^{+}/ETS-4 and Cd^{2+}/Na^{+}/ETS-10, has been performed using MS equations for mass transport inside the particle. With this approach, the MS diffusivity of the common Na^{+}/Cd^{2+} pair ($Đ_{Na^{+},Cd^{+}}$) was fixed in both systems. Additionally, the two external convective mass transfer coefficients (k_f) were interrelated by an appropriate correlation in order to fit only one k_f to the experimental data.

This work has been developed in the period from November 2011 to July 2012 in Associate Laboratory CICECO—Department of Chemistry, University of Aveiro, Portugal.

Materials and methods

Nernst–Planck based model

Ion exchange may be represented by a conventional chemical equilibrium between two counter ions (Helfferich 1995). When the solid is initially in B form and A is the counter ion in solution, one writes as follows:

$$z_A\overline{B^{z_B}} + z_B A^{z_A} \Leftrightarrow z_B\overline{A^{z_A}} + z_A B^{z_B} \qquad (1)$$

being z_A and z_B the electrochemical valences, and the upper bars identify the solid phase.

An electric field in an electrolyte solution, caused by the different mobilities of counter ions, produces an additional force responsible for the transference of ions. In this case, the flux of each counter ion in dilute ionic solutions may be described by the NP equations (Helfferich 1995):

$$N_{\mathrm{A}} = -D_{\mathrm{A}}\left(\frac{\partial q_{\mathrm{A}}}{\partial r}\right) - D_{\mathrm{A}} z_{\mathrm{A}} q_{\mathrm{A}} \frac{F}{\Re T}\left(\frac{\partial \varphi}{\partial r}\right) \tag{2}$$

$$N_{\mathrm{B}} = -D_{\mathrm{B}}\left(\frac{\partial q_{\mathrm{B}}}{\partial r}\right) - D_{\mathrm{B}} z_{\mathrm{B}} q_{\mathrm{B}} \frac{F}{\Re T}\left(\frac{\partial \varphi}{\partial r}\right) \tag{3}$$

where D_{A} and D_{B} are the self-diffusion coefficients of species A and B, q_{A} and q_{B} are the molar concentration of counter ions in the particle, F is Faraday constant, $\Re$ is gas constant, T is absolute temperature, ϕ is the electrostatic potential and r is the radial position. Assuming the particle is subjected to the restrictions of electroneutrality and nonexistent electric current, the following relations has to be considered:

$$q_{\mathrm{A}} z_{\mathrm{A}} + q_{\mathrm{B}} z_{\mathrm{B}} = Q \tag{4}$$

$$z_{\mathrm{A}} N_{\mathrm{A}} + z_{\mathrm{B}} N_{\mathrm{B}} = 0 \tag{5}$$

with Q the ion exchanger capacity. In order to eliminate the electrostatic potential term in the transport equations, Eqs. (2) and (3) may be substituted into Eq. (5):

$$\frac{F}{\Re T}\frac{\partial \phi}{\partial r} = \frac{z_{\mathrm{A}}(D_{\mathrm{B}} - D_{\mathrm{A}})}{z_{\mathrm{A}} q_{\mathrm{A}}(z_{\mathrm{A}} D_{\mathrm{A}} - z_{\mathrm{B}} D_{\mathrm{B}}) + D_{\mathrm{B}} z_{\mathrm{B}} Q}\frac{\partial q_{\mathrm{A}}}{\partial r} \tag{6}$$

and after combination with Eq. (2), the general expression for the flux of A is obtained:

$$N_{\mathrm{A}} = -\frac{D_{\mathrm{A}} D_{\mathrm{B}}(z_{\mathrm{B}}^2 q_{\mathrm{B}} + z_{\mathrm{A}}^2 q_{\mathrm{A}})}{D_{\mathrm{A}} z_{\mathrm{A}}^2 q_{\mathrm{A}} + D_{\mathrm{B}} z_{\mathrm{B}}^2 q_{\mathrm{B}}}\left(\frac{\partial q_{\mathrm{A}}}{\partial r}\right) \tag{7}$$

This equation may be written as a special form of the Fick's first law with a coupled interdiffusion coefficient, D_{AB}:

$$N_{\mathrm{A}} = -D_{\mathrm{AB}}\left(\frac{\partial q_{\mathrm{A}}}{\partial r}\right) \text{ and } D_{\mathrm{AB}} \equiv \frac{D_{\mathrm{A}} D_{\mathrm{B}}(z_{\mathrm{A}}^2 q_{\mathrm{A}} + z_{\mathrm{B}}^2 q_{\mathrm{B}})}{D_{\mathrm{A}} z_{\mathrm{A}}^2 q_{\mathrm{A}} + D_{\mathrm{B}} z_{\mathrm{B}}^2 q_{\mathrm{B}}} \tag{8}$$

Maxwell–Stefan based model

In the following, surface diffusion will be assumed as the transport mechanism of counter ions, since due to the significantly small pore diameters of ETS-4 and ETS-10, ions never escape from the force field of the matrix co-ions, mainly owing the strong and long-range nature of the electrostatic interactions. Assuming the solid phase as a uniform distribution of fixed ionic charges corresponding to the $(n+1)$th component, through which counter ions diffuse, $u_{n+1} = 0$ as in the well-known Dusty Gas Model (Jackson 1977; Krishna and Wesselingh 1997). Accordingly, the MS transport equation for species i in multicomponent isothermal ionic systems is (Krishna and Wesselingh 1997; Silva and Lito 2007; Lito and Silva 2008; Lito et al. 2012, 2013):

$$-\nabla\mu_i - F z_i \nabla\varphi = \sum_{\substack{j=1\\ j\neq i}}^{n} \frac{y_j \Re T(u_i - u_j)}{Đ_{ij}} + \frac{y_s \Re T u_i}{Đ_{is}} \tag{9}$$

where $\nabla\mu_i$ is the chemical potential gradient of i, z_i is the charge of component i, $Đ_{ij}$ is the MS surface diffusivity of pair i–j, $Đ_{is}$ is the MS surface diffusivity corresponding to the interaction between i and the fixed ionic charges (subscript s stands for solid), $y_j = q_j/q_{\mathrm{t}}$ is molar fraction of counter ion j, $y_{\mathrm{s}} = Q/q_{\mathrm{t}}$ is molar fraction of fixed charged groups, q_j is the molar concentration of j, and q_{t} is the total concentration of ionic species, and u_i and u_j are the velocities of i and j relative to the solid. It should be noted that $\sum_{i=1}^{n+1} y_i = 1$, and q_{t} is not constant whenever counter ions have different electrochemical valences. Here n is the number of counter ions, and so, the solid corresponds to the $(n+1)$th component of the mixture. Taking into account the definition of molar flux of the ionic species j, i.e. $N_j = q_{\mathrm{t}} y_j u_j$, Eq. (9) may be recast as follows:

$$-\frac{y_i}{\Re T}\nabla\mu_i - y_i z_i \frac{F}{\Re T}\nabla\varphi = \sum_{\substack{j=1\\ j\neq i}}^{n} \frac{y_j N_i - y_i N_j}{q_{\mathrm{t}} Đ_{ij}} + \frac{y_{\mathrm{s}} N_i}{q_{\mathrm{t}} Đ_{is}} \tag{10}$$

Assuming instantaneous equilibrium between surface and a (hypothetical) solution of composition x_i^*, one writes $\mu_i = \mu_{i,\mathrm{eq.sol}}$. Furthermore, since gradient $\nabla\mu_i$ corresponds to $\nabla\mu_{i,\mathrm{eq.sol}}$, one may finally equate as follows:

$$\frac{y_i}{\Re T}\nabla\mu_i = \sum_{j=1}^{n} \Gamma_{ij}\nabla y_j \quad \text{with } \Gamma_{ij} \equiv y_i \frac{\partial \ln(\gamma_{i,\mathrm{eq.sol}} x_i^*)}{\partial y_j} \tag{11}$$

where $\gamma_{i,\mathrm{eq.sol}}$ is the activity coefficient of counter ion i in the solution under equilibrium, Γ_{ij} is called thermodynamic factor. It is worth noting that in Eq. (11), x_i^* and y_i are related by the equilibrium isotherm.

Equation (10) can be expressed in n-dimensional matrix notation. Introducing the matrix of thermodynamic factors, $[\Gamma]$, given by Eq. (11), one obtains the following:

$$(N) = -q_{\mathrm{t}}[B]^{-1}[\Gamma](\nabla y) - q_{\mathrm{t}}[B]^{-1}(\nabla\xi) \tag{12}$$

where

$$B_{ii} = \frac{y_{\mathrm{s}}}{Đ_{is}} + \sum_{\substack{j=1\\ j\neq i}}^{n} \frac{y_j}{Đ_{ij}}, \quad B_{ij} = -\frac{y_i}{Đ_{ij}} \tag{13}$$

$$\nabla\xi_i = y_i z_i \frac{F}{\Re T}\nabla\phi \tag{14}$$

Under conditions of electroneutrality and nonexistent electric current, the following relations are adhered to

$$\sum_{i=1}^{n+1} q_i z_i = 0 \tag{15}$$

$$\sum_{i=1}^{n+1} z_i N_i = 0 \tag{16}$$

Equations (12) and (16) may be combined to eliminate $\nabla\phi$ from the generalized MS equations, being the following relation obtained

$$\frac{F}{\Re T}\nabla\phi = \frac{-\sum_{i=1}^{n} z_i\left(\sum_{j=1}^{n} L_{ij}\nabla y_j\right)}{\sum_{i=1}^{n} y_i z_i\left(\sum_{i=1}^{n} z_j L_{ji}\right)} \tag{17}$$

For the particular case of the systems studied in this work, we assumed that the co-ions are excluded from the zeolite particles (Donnan exclusion) and that the liquid solution is ideal.

Material balances, initial and boundary conditions, and equilibrium isotherms

The mass balances in a spherical particle and in a perfectly stirred reservoir, neglecting liquid and solid volume changes, are represented by, respectively, the following:

$$\left(\frac{\partial q_{\mathrm{A}}}{\partial t}\right) = -\frac{1}{r^2}\frac{\partial}{\partial r}\left(r^2 N_{\mathrm{A}}\right) \tag{18}$$

$$\frac{\mathrm{d}C_{\mathrm{A}}}{\mathrm{d}t} = -\frac{V_{\mathrm{s}}}{V_{\mathrm{L}}}\frac{\mathrm{d}\bar{q}_{\mathrm{A}}}{\mathrm{d}t} \tag{19}$$

where the average loading per unit particle volume is calculated as follows:

$$\bar{q}_{\mathrm{A}} = \frac{3}{R^3}\int_0^R r^2 q_{\mathrm{A}}\mathrm{d}r \tag{20}$$

Here R, V_{s}, and V_{L} are the particle radius, volume of solid phase, and volume of fluid phase, respectively, and C_{A} is the molar concentration of i in bulk solution.The previous differential equations will be subject to the following initial conditions (no B in solution, no A in solid):

$$t = 0, \quad \begin{cases} q_{\mathrm{A}} = \bar{q}_{\mathrm{A}} = 0 \\ C_{\mathrm{A}} = C_{\mathrm{A},0} \end{cases} \tag{21}$$

and the boundary conditions specify the interface concentration and the null central flux:

$$r = R, \quad q_{\mathrm{A}} = q_{\mathrm{A,R}} \tag{22}$$

$$r = 0, \quad \left(\frac{\partial q_{\mathrm{A}}}{\partial r}\right) = 0 \tag{23}$$

Assuming that both film and intraparticle mass transfer resistances exist, the concentration at the interface is determined by equalizing internal diffusion and film convection fluxes, i.e.:

$$N_{\mathrm{A}}|_{r=R} = k_{\mathrm{f}}\left(C_{\mathrm{A}} - C_{\mathrm{A,R}}\right) \tag{24}$$

For well-established agitated systems, k_{f} may be estimated using correlations which generally depend on the Reynolds, Schmidt, and Power numbers and on geometrical parameters such as the ratio of impeller to tank diameter, the specific geometry of the impeller, and the geometry of baffling, if any, used to inhibit vortex formation in the vessel (Treybal 1981; Misic et al. 1982; Kulov et al. 1983; Miller et al. 1984; Slater 1991). The correlation of Armenante and Kirwan (1989) may be used to estimate the convective mass transfer coefficient for microparticles in agitated systems:

$$Sh = 2 + 0.52Re^{0.52}Sc^{1/3} \tag{25}$$

where $Sh = k_{\mathrm{f}}d_{\mathrm{p}}/D_{\mathrm{Aw}}$ is the Sherwood number, d_{p} is the particle diameter, D_{Aw} is the diffusivity of the solute in solution, $Re = \varepsilon^{1/3}d_{\mathrm{p}}^{4/3}/\nu$ is the Reynolds number, ε is the mixer power input per unit of fluid mass, ν is the kinematic viscosity, and $Sc = \nu/D_{\mathrm{Aw}}$ is the Schmidt number.

The equilibrium between bulk solution and exchanger is evaluated in this work using the Langmuir–Freundlich (LF) isotherm. The LF isotherm involves parameters $q_{\max}$, K_{LF}, and n_{LF}, being given by the following:

$$q_{\mathrm{A}} = \frac{q_{\max}K_{\mathrm{LF}}C_{\mathrm{A}}^{1/n_{\mathrm{LF}}}}{1 + K_{\mathrm{LF}}C_{\mathrm{A}}^{1/n_{\mathrm{LF}}}} \tag{26}$$

The LF isotherm parameters used in this work were obtained by fitting experimental data of cadmium(II) sorption in ETS-10 (Camarinha et al. 2009) and ETS-4 (Barreira et al. 2009) and are compiled in Table 1, being q_{A}, $q_{\max}$, and C_{A} expressed in eq/m^3. The equilibrium curves are shown in Fig. 1 together with the corresponding experimental data.

Numerical solution

The simultaneous solution of the set of differential and algebraic equations listed above gives the concentration of counter ions in the fluid and their concentration profiles in the solid phase as function of position and time. The model has been solved numerically according to the following procedure:

1. The MS flux N_{A} was obtained by substituting Eqs. (13), (14), and (17) in Eq. (12). Then, it was substituted in the material balance, Eq. (18), giving rise to first- and second-order spatial derivatives.
2. The differential equations for the solid were numerically solved using the Method of Lines (Schiesser

Table 1 Langmuir–Freundlich isotherm parameters for cadmium(II) in ETS-10 (Camarinha et al. 2009) and ETS-4 (Barreira et al. 2009), obtained at 295 K

Langmuir–Freundlich			
	K_{LF} $\left(\mathrm{m}^{3/n}\,\mathrm{eq}^{-1/n}\right)$	$q_{\max}$ $\left(\mathrm{eq\ m}^3\right)$	$1/n$
ETS-10	4.130×10^3	3.629×10^3	1.06
ETS-4	1.771×10^3	7.828×10^3	1.14

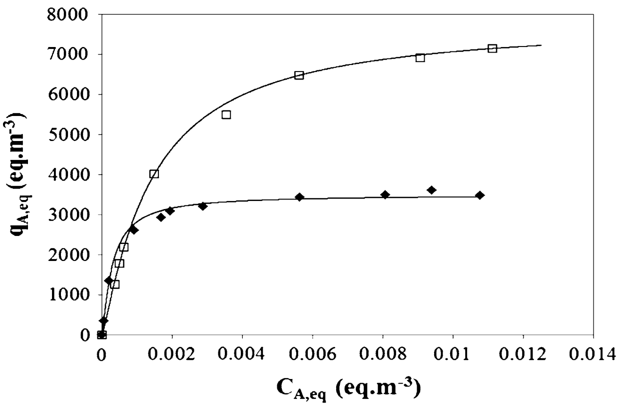

Fig. 1 Equilibrium data of Cd^{2+} removal by ETS-4 (Barreira et al. 2009) and ETS-10 (Camarinha et al. 2009) at pH = 6 and $T = 295$ K, along with Langmuir–Freundlich isotherms fitted. Symbols: *squares* ETS-4 (Barreira et al. 2009), *lozenges* ETS-10 (Camarinha et al. 2009), *solid lines* Langmuir–Freundlich isotherms fitted

   1991) and integrated by the finite-difference approach; the radial position has been discretized into 31 nodes, since no accuracy enhancement was observed using a larger number of nodes; it only increased time-consuming of simulation. Central differences of second-order were applied to the central nodes, while second-order forward and backward difference formulas were adopted for the first and last nodes, respectively. The boundary conditions given by Eqs. (22) and (23) were used in the last and first nodes, respectively. Equation (24) was applied after substitution of the inverted isotherm, i.e. from Eq. (26) one gets $C_{A,R} = C_{A,R}(q_{A,R})$.
3. The final model equations, (18) and (19), were integrated using the Ode15s function of Matlab, where the average loading per unit particle volume (Eq. 20) was numerically evaluated using the 1/3 Simpson's Rule. This took approximately 18 s.
4. The diffusion and the convective mass transfer coefficients are the model parameters to fit the experimental data. The Nelder–Mead simplex direct search algorithm was used to optimize them, by adopting the sum of squared deviations as objective function: $\chi^2 = \sum \left(C_{A,\exp,i} - C_{A,i}\right)^2$.

Table 3 Physical properties of ETS-4 and ETS-10 titanosilicates

	ETS-4	ETS-10
Formula	$[Na_9Ti_5Si_{12}O_{38}(OH)\cdot 12H_2O]$	$[(Na,K)_2TiSi_5O_{13}\cdot 4H_2O]$
Density (kg/m$^{3)}$	2,200	1,800
Ion exchanger capacity (eq/kg)	6.39	4.52
Particle diameter (10^{-6} m)	0.5–0.9	5
Pore diameter (10^{-10} m)	3–4	4.9 × 7.6

Sources of experimental ion exchange data

The experimental data used to examine the model studied in this essay concerns batch experiments where cadmium(II) is removed from aqueous solution using ETS-4 and ETS-10 microporous titanosilicates, both in Na form [data from Barreira et al. (2009) and Camarinha et al. (2009), respectively]. The experiments were carried out in powder form at fixed temperature, solution pH, and initial concentration, using different titanosilicate masses. Totally, eleven experiments are considered, corresponding to the conditions listed in Table 2. In those works, the bulk concentration of Cd^{2+} has been measured along time. Table 3 compiles relevant physical properties of ETS-4 and ETS-10 particles used in the experiments. In the following, subscript A denotes Cd^{2+} and subscript B symbolizes Na^+.

Results and discussion

This section starts with a brief discussion of the experimental curves selected for modelling. Then, the calculated results are presented and analyzed in detail. The correlated kinetic curves and the predicted concentration profiles inside the particle are given and discussed individually. Finally, the predictive capability of the model under research is evaluated.

Brief discussion of the experimental kinetic curves

An exhaustive discussion about the behaviour of the experimental kinetic curves and the influence of the mass

Table 2 Experimental conditions of data used in calculations for Cd^{2+} removal by ETS-4 (Barreira et al. 2009) and ETS-10 (Camarinha et al. 2009). Fixed: $T = 295 \pm 1$ K; $V_L = 2 \times 10^{-3}$ m^3; pH = 6; $C_{A,0} = 0.85 \times 10^{-3}$ kg/m^3

ETS-4	Experiment no.	1	2	3					
	Mass of ETS-4, 10^{-6} kg	4.3	25.0	50.3					
ETS-10	Experiment no.	4	5	6	7	8	9	10	11
	Mass of ETS-10, 10^{-6} kg	5	7.5	10	15.2	17.5	20	40	160

of titanosilicates upon their trend has been given elsewhere (Barreira et al. 2009; Camarinha et al. 2009). Here we highlight only the main results and conclusions.

Figure 2a, b shows the evolution of normalized Cd^{2+} concentration in the fluid along time, measured, respectively, for different ETS-4 and ETS-10 masses at pH 6 (Experiments 1–3, and 4–11 of Table 2). Results follow the expected trend, i.e., cadmium removal increases with increasing titanosilicate mass since the ion exchange capacity is proportional to the solid mass. All curves exhibit a fast initial metal uptake followed by the characteristic slower removal toward the equilibrium. Such behaviour is due to the large driving force for ions transport at beginning of the process, since both ETS-4 and ETS-10 particles are initially free of Cd^{2+}. For ETS-4, the uptake equilibrium was attained in about 30 h (Fig. 2a), whereas only 3 h was sufficient for ETS-10 (Fig. 2b). Such results are due to the pore diameters of these materials, i.e., 0.49 × 0.76 nm (ETS-10) and 0.3–0.4 nm (ETS-4). Since ETS-10 pores are wider, cadmium(II) is expected to diffuse faster through the solid matrix. It is important to detach that pH remains constant along time (pH 6), which is fundamental to ensure that we are on the presence of a binary ion exchange between Cd^{2+} and the titanosilicate counter ion.

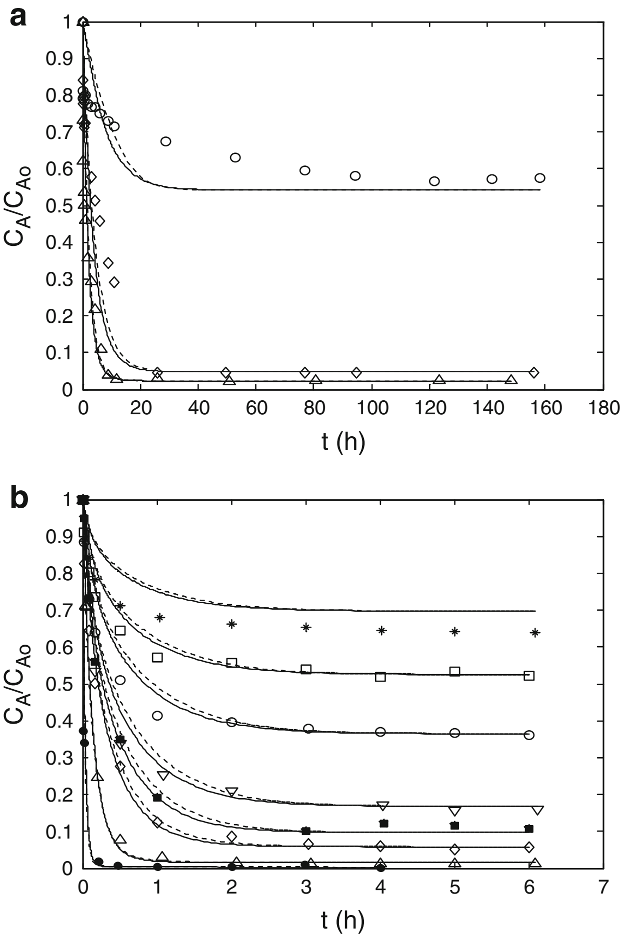

Fig. 2 Plot of the normalized concentration of Cd^{2+} in the bulk solution versus time: modelling and experimental data for Cd^{2+} removal **a** by ETS-4 (Barreira et al. 2009); experimental conditions (see Table 2): *open circle* Exp.1; *open diamond* Exp.2; *open triangle* Exp.3; and **b** by ETS-10 (Camarinha et al. 2009); experimental conditions (see Table 2): *asterisk* Exp.4, *open square* Exp.5, *open circle*, Exp.6, *open inverted triangle* Exp.7, *filled square* Exp.8, *open diamond* Exp.9, *open triangle* Exp.10, *filled circle* Exp.11. *Full lines* MS-based model (this work), *dashed lines* NP-based model (from Barreira et al. 2009; Camarinha et al. 2009)

Calculated results and modelled kinetic curves

The uptake curves represented by the MS-based model are plotted against time in Fig. 2a, b, along with experimental data. In Table 4, the calculated parameters (MS diffusivities and convective mass transfer coefficients) and statistical analysis of regression and parameters are listed together with the corresponding average absolute relative deviations (AARD) found. The experimental data measured after achieving ion exchange equilibrium (i.e. the horizontal branches of both figures) were taken to estimate the experimental variance. Both figures show a good agreement between model results and experimental data, confirmed by the low deviation found, AARD = 15.3%, mainly if one takes into account that (1) the data refer to two sets of independent and distinct systems, (2) the coefficient $Đ_{AB}$ was fixed in both systems, and (3) the two values of k_f were related by Eq. (25), which means that only one parameter was fitted. An accurate correlation was found in both cases even in the transition from the steep descent to the horizontal branch, where kinetic curves are frequently difficult to fit. In fact, this may be considered a remarkable result, attending to the number of experimental curves fitted (eleven in the whole), to the different sorbents (ETS-4 and ETS-10) simultaneously analyzed, and to the discrepancy of the masses of titanosilicates used (which varies from 4.3 to 50.3 mg of ETS-4, and 5 to 160 mg of ETS-10).

The MS diffusivities of the pairs Cd^{2+}/ETS-4 fixed ionic charges and Cd^{2+}/ETS-10 fixed ionic charges (i.e. $Đ_{As,1}$ and $Đ_{As,2}$) differ by around three orders of magnitude, which point out the different interactions between each ion and titanosilicate (1.039×10^{-19} vs. 7.708×10^{-16} m^2s). The same behaviour was found for MS diffusivities of Na^+/fixed ionic charges pairs ($Đ_{As,1} = 9.073 \times 10^{-19}$ and $Đ_{Bs,2} = 9.181 \times 10^{-15}$ m^2s). In fact, this is an expected result because it comes from the difference between the pore dimensions of both materials (i.e. 0.3–0.4 and 0.49 × 0.76 nm, for ETS-4 and ETS-10 respectively). Since ETS-10 pores are wider, cadmium and sodium cations are expected to diffuse through it with higher mobility. In the whole, the orders of magnitude of the calculated MS diffusivities are consistent with the small pore diameters of ETS-4 and ETS-

Table 4 Calculated results with the MS-based model of this work: parameters optimized, average absolute relative deviation, and statistical analysis

Maxwell–Stefan model: AARD = 15.3 %

Parameter	Estimative	Standard deviation	Confidence interval	*t* test
$Đ_{\mathrm{A,ETS\text{-}10}}$ (m^2/s)	7.708×10^{-16}	1.274×10^{-16}	5.199×10^{-16}–1.022×10^{-15}	6.048
$Đ_{\mathrm{B,ETS\text{-}10}}$ (m^2/s)	9.181×10^{-15}	2.369×10^{-15}	4.517×10^{-15}–1.385×10^{-14}	3.876
$Đ_{\mathrm{A,ETS\text{-}4}}$ (m^2/s)	1.039×10^{-19}	8.775×10^{-22}	1.022×10^{-19}–1.057×10^{-19}	1.184×10^{2}
$Đ_{\mathrm{B,ETS\text{-}4}}$ (m^2/s)	9.073×10^{-19}	7.340×10^{-20}	7.628×10^{-19}–1.052×10^{-18}	1.236×10^{1}
$Đ_{\mathrm{AB}}$ (m^2/s)[a]	1.486×10^{-16}	3.391×10^{-18}	1.419×10^{-16}–1.553×10^{-16}	4.383×10^{1}
$k_{f,\mathrm{ETS-10}}$ (m/s)[b]	1.014×10^{-4}	2.259×10^{-6}	9.690×10^{-5}–1.058×10^{-4}	4.486×10^{1}
$k_{f,\mathrm{ETS-4}}$ (m/s)[b]	6.104×10^{-4}			

[a] $Đ_{\mathrm{AB}}$ was made equal in both systems

[b] The relation between both values of k_{f} (Eq. 27) was assumed during calculations, so only one k_{f} was fitted

10, and the strong and long-range nature of the electrostatic interactions. In the literature, very small diffusivities are usually found for ions inside microporous materials, as for instance, 1.14×10^{-17} and 1.96×10^{-21} m^2/s for Na$^+$ and K$^+$ in analcite, respectively, 1.8×10^{-17} and 8.0×10^{-18} m^2/s for Ca^{2+} and Mg^{2+} in semi-crystalline zeolite-NaA, and 1.11×10^{-19} m^2/s for Hg^{2+} in ETS-4.

The convective mass transfer coefficient can be estimated by Armenante and Kirwan's correlation. Even though some of its parameters were not entirely appropriate (e.g. the power was approximately calculated, and the size of ETS-4 particles ($d_{\mathrm{p}} = 0.7 \times 10^{-6}$ m) was one order of magnitude lower than the inferior limit studied by Armenante and Kirwan (range of $d_{\mathrm{p}} = 6$–420×10^{-6} m), this correlation may still be applied to achieve reliable results. Furthermore, as established in Eq. (25), the following relation connects both k_{f}'s:

$$k_{\mathrm{f,ETS-4}} = k_{\mathrm{f,ETS-10}} \times \frac{d_{\mathrm{p,ETS-10}}}{d_{\mathrm{p,ETS-4}}} \times \frac{2 + a \times d_{\mathrm{p,ETS-4}}^{4/3 \times 0.52}}{2 + a \times d_{\mathrm{p,ETS-10}}^{4/3 \times 0.52}} \tag{27}$$

where $a = 0.52 \times \varepsilon^{0.52/3} \times \nu^{1/3-0.52} \times D_{\mathrm{Aw}}^{-1/3}$. In this way, one reduces the optimized mass transfer coefficients to $k_{\mathrm{f,ETS-10}}$.

In Table 4, the standard errors and confidence intervals at 95 % of the MS model parameters show that diffusivities of counter ions through ETS-10 are less accurate than the remaining parameters. Particularly welcome is the fact that the regression of $Đ_{\mathrm{AB}}$ and $k_{\mathrm{f,ETS-10}}$ provided low deviations ($1.486 \times 10^{-16} \pm 3.391 \times 10^{-18}$ and $1.014 \times 10^{-4} \pm 2.259 \times 10^{-6}$, respectively) if ones take into account that their fitting is intimately linked to both sets of data (ETS-4 and ETS-10). Furthermore, the significance two-sided *t* test at 95 % confirms that all parameters are statically non-zero since they are higher than the calculated reference ($t = 1.969$). From an analysis of variance of our MS model, it is possible to conclude that the model is able to take the variability of the experimental data into account. The calculated ratio between the mean squares due to model and residuals gave 5.3×10^4, which is absolutely higher than the tabulated *F* for 95 % with 5 and 128 degrees of freedom. Hence, the model is statistically significant to represent the experimental data of the ion exchange uptake curves.

Figure 3 represents the normalized concentration of cadmium(II) in ETS-4 along time and radial position, for Experiment 1 of Table 2. Similar behaviour is found for the remaining ones. This plot illustrates an interesting time evolution of normalized concentration at surface, $q_{\mathrm{A}}(t; r = R)/q_{\mathrm{A,eq}}$. In particular, the initial sudden increase in surface concentration is so pronounced that it passes through a maximum and then decreases gradually until the equilibrium. In contrast, inside particle and far from the surface, the concentration increases monotonously. A simple form to interpret these findings is the following. In the absence of film resistance, the initial particle concentration at surface would suddenly increase from $q_{\mathrm{A}}(t = 0^-, r = R) = 0$ to $q_{\mathrm{A}}(t = 0^+, r = R) = q_{\mathrm{A}}(C_{\mathrm{A0}})$, i.e. to the concentration in equilibrium with initial bulk solution. Subsequently, $q_{\mathrm{A}}(t, r = R)$ would decrease monotonously until final system equilibration, i.e. $q_{\mathrm{A}}(t, r) \to q_{\mathrm{A,eq}} = q_{\mathrm{A}}(t = \infty, r)$, because the ion exchange progresses and thus the bulk concentration decreases along time. Accordingly, the normalized concentration at surface may attain values higher than one. Nonetheless, in a real case, the existence of external diffusion smoothes the ideal trend identified with such initial step increase, as illustrated in Fig. 3. The same behaviour was found for ETS-10, and hence, it has been omitted in the discussion.

Figure 2a, b also shows a comparison between the results obtained using our MS model (full lines) and the results achieved independently by Barreira et al. (2009) (ETS-4, Fig. 2a) and Camarinha et al. (2009) (ETS-4, Fig. 2b) with the NP-based model (dashed lines). Table 5 compiles the corresponding NP self-diffusion coefficients, the mass transfer coefficient, and average absolute relative

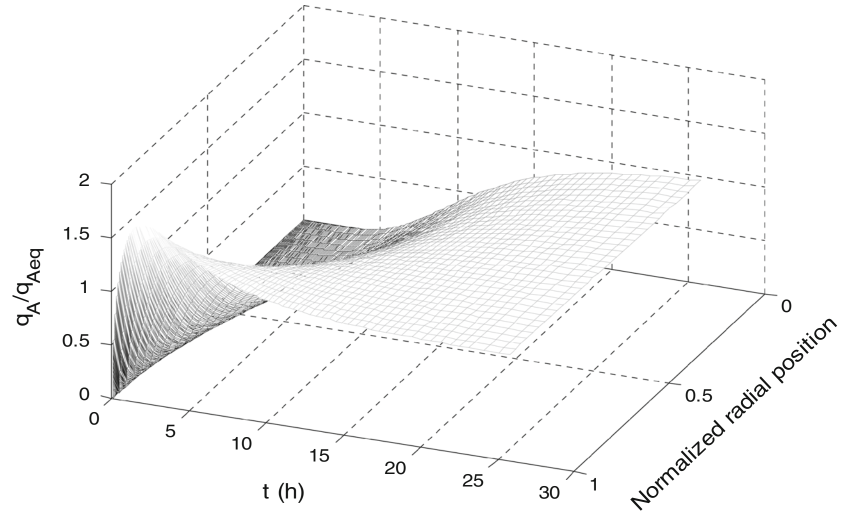

Fig. 3 Simulation normalized concentration of the particle as function of time and normalized radial position for Experiment 1 (Table 2)

Table 5 Calculated results with the NP-based model: parameters optimized and average absolute relative deviation obtained by Barreira et al. (2009) and Camarinha et al. (2009)

Nernst–Planck				
	D_A (m^2/s)	D_B (m^2/s)	k_f (m/s)	AARD (%)
ETS-10[a]	1.082×10^{-16}	2.319×10^{-15}	1.628×10^{-4}	11.9
ETS-4[b]	4.548×10^{-19}	5.246×10^{-18}	1.281×10^{-3}	17.2

[a] Camarinha et al. (2009)

[b] Barreira et al. (2009)

deviations. It is evident from Fig. 2 the similar fitting capability of both models, which can be confirmed by the similar deviations found ($\mathrm{AARD_{MS}} = 15.3\,\%$ vs. $\mathrm{AARD_{NP}} = 17.2\,\%$ and $\mathrm{AARD_{NP}} = 11.9\,\%$ for ETS-4 and ETS-10, respectively). Nonetheless, it is important to point out that all the eleven curves (corresponding to distinct materials) have been here simultaneously fitted, while for the NP-based model, the ETS-4 and ETS-10 results were separately correlated. The fact that both models are approximately indistinguishable under the range of experimental conditions studied is fundamental for the validation of this MS approach, since it implies that our model obeys the low concentration solutions limit. From the literature, it is well known that NP is not adequate at high concentrations, while MS can provide accurate and meaningful representations. In terms of time-consuming, the MS simulations require around 6 times more than NP approach, which can be attributed to the inferior complexity of NP equations once the numerical approach was the same in both cases.

The diffusion coefficients optimized with both models (Tables 4, 5) possess the same order of magnitude, even though MS and NP diffusivities have distinct intrinsic physical meaning: while MS diffusivities describe the interaction between each pair of species, including the solid fixed ionic charges, NP self-diffusion coefficients uniquely represent the mobility of each counter ion in the ion exchanger.

The predictive capability of the MS-based model was also analyzed in this work. Accordingly, the parameters involved ($\text{Đ}_{\mathrm{As},1}$, $\text{Đ}_{\mathrm{As},2}$, $\text{Đ}_{\mathrm{Bs},1}$, $\text{Đ}_{\mathrm{Bs},2}$, Đ_{AB}, k_f) were optimized using three sets of experimental data obtained with EST-4 (Experiments 1–3 of Table 2) and another three sets of data from ETS-10 (Experiments 5–7 of Table 2); afterwards, the remaining five curves were predicted with those parameters. The results accomplished are plotted in Fig. 4, in $C_A/C_{A,0}\,(\text{predicted})$ versus $C_A/C_{A,0}\,(\text{fitted})$ form. The approximate linearity observed between predicted and correlated values highlights the model ability to predict ion exchange behaviour under different experimental conditions, including diverse ion exchange materials. This skill may be ascribed to the binary nature of the MS diffusivities, which represent the interaction between each pair of species, independently of the remaining components present in the system.

Conclusion

In this essay, modelling of ion exchange kinetics was carried out using the MS equations for the ionic transport

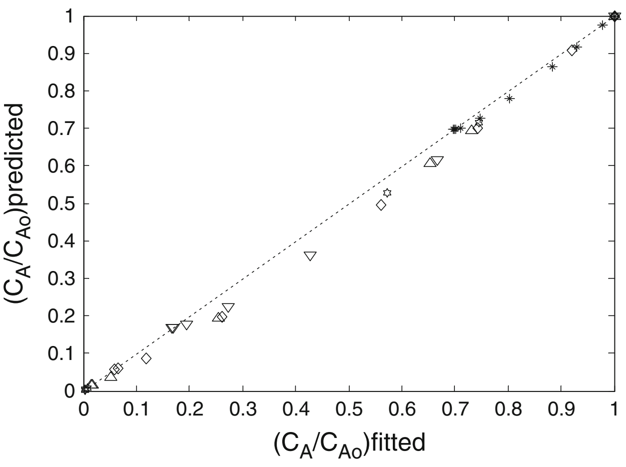

Fig. 4 Comparison between predicted and fitted Cd^{2+} concentration in solution by MS-based model. *Symbols* are the same as in Fig. 2b

inside the particle exchanger. The performance of this model was investigated with independent data published for Cd^{2+} removal from aqueous solutions using two microporous titanosilicates, namely ETS-4 and ETS-10. The MS diffusivities and convective mass transfer coefficients are the parameters and have been simultaneously optimized in order to test model ability to describe data measured under very different conditions and for distinct ionic systems (Cd^{2+}/Na^{+}/ETS-4 and Cd^{2+}/Na^{+}/ETS-10). In the whole, the model accomplished good representation of the experimental data (average deviation of 15.3 %), since eleven sets of data were fitted together, and two parameters were eliminated by taking into account the nature of the systems and experiment conditions. Furthermore, the fine predictive capability of the MS-based model has been highlighted, since it was able to predict several uptake curves using parameters optimized from some independent curves.

Acknowledgments Patrícia F. Lito wishes to thank Fundação para a Ciência e Tecnologia (Portugal) for the Grant (SFRH/BPD/63214/2009) provided for this study.

Nomenclature

A	External particle surface area (m)
AARD	Average absolute relative deviation
$[B]$	Matrix with MS diffusivities
C_i	Molar concentration of i in bulk solution (mol/m^3)
d_p	Particle diameter (m)
D_i	Self-diffusion coefficient of species i (m^2/s)
D_{Aw}	Diffusivity of the solute in solution (m^2/s)
D_{ij}	Interdiffusion coefficient of pair i–j (m^2/s)
$Đ_{ij}$	MS surface diffusivity of pair i–j (m^2/s)
$Đ_{is}$	MS surface diffusivity of pair i-fixed ionic charges (m^2/s)
F	Faraday constant (C/mol)
k_f	Film mass transfer coefficient (m/s)
K_{LF}	Langmuir–Freundlich parameter
$[L]$	$= [B]^{-1}$
n	Langmuir–Freundlich parameter
N_j	Molar flux of counter ion j (mol/m^2 s)
q_j	Molar concentration of counter ion j in the particle, (mol/m^3)
q_t	Total concentration of ionic species in the particle (mol/m^3)
$\bar{q}_j$	Average concentration of j in the particle (mol/m^3)
Q	Ion exchanger molar capacity (mol/m^3)
r	Radial position in the particle (m)
Sc	Schmidt number
Sh	Sherwood number
$\Re$	Gas constant (J/mol K)
R	Particle radius (m)
Re	Reynolds number
t	Time, s (and h in the figures)
T	Absolute temperature (K)
u_i	Velocity of i relative to the solid, (m/s)
V_L	Volume of fluid phase (m^3)
V_s	Volume of solid phase (m^3)
x_i	Molar fraction of i in bulk solution
y_j	Molar fraction of counter ion j in the particle
z_i	Charge of component i

Greek letters

ε	Mixer power input per unit of fluid mass
$\gamma_{i,sol}$	Activity coefficient of counter ion i in a solution in equilibrium with particle
φ	Electrostatic potential (V)
$[\Gamma]$	Matrix of thermodynamic factors
ξ_i	Related with the electrostatic potential gradient
ν	Kinematic viscosity
μ_i	Chemical potential of i (J/mol)

Subscripts

A	Counter ion initially present in bulk solution (Cd^{2+})
B	Counter ion initially present in particle (Na^{+})
S	Fixed charged groups of the particle
∞	Final equilibrium condition of experiment

References

Armenante PM, Kirwan DJ (1989) Mass-transfer to microparticles in agitated systems. Chem Eng Sci 44(12):2781–2796

Barreira LD, Lito PF, Antunes BM, Otero M, Lin Z, Rocha J, Pereira E, Duarte AC, Silva CM (2009) Effect of pH on cadmium(II) removal from aqueous solution using titanosilicate ETS-4. Chem Eng J 155(3):728–735

Camarinha ED, Lito PF, Antunes BM, Otero M, Lin Z, Rocha J, Pereira E, Duarte AC, Silva CM (2009) Cadmium(II) removal from aqueous solution using microporous titanosilicate ETS-10. Chem Eng J 155(1–2):108–114

Chanda M, Rempel GL (1995) Sorption of sulfide on a macroporous, quaternized poly(4-vinyl pyridine) in alkaline medium. React Polym 24(3):203–212

Choi JH, Kim SD, Kwon YJ, Kim WJ (2006) Adsorption behaviors of ETS-10 and its variant, ETAS-10 on the removal of heavy metals, Cu^{2+}, Co^{2+}, Mn^{2+} and Zn^{2+} from a waste water. Microporous Mesoporous Mater 96(1–3):157–167

Cincotti A, Mameli A, Locci AM, Orru R, Cao G (2006) Heavy metals uptake by Sardinian natural zeolites: experiment and modeling. Ind Eng Chem Res 45(3):1074–1084

Clark RB, Frid C, Attrill M (2001) Marine pollution. Oxford press, Oxford

Dabrowski A, Hubicki Z, Podkoscielny P, Robens E (2004) Selective removal of the heavy metal ions from waters and industrial wastewaters by ion-exchange method. Chemosphere 56(2):91–106

Dolgonosov AM, Khamizov RK, Krachak AN, Prudkovsky AG (1995) Macroscopic model for multispecies ion-exchange kinetics. React Funct Polym 28(1):13–20

Ferreira TR, Lopes CB, Lito PF, Otero M, Lin Z, Rocha J, Pereira E, Silva CM, Duarte A (2009) Cadmium(II) removal from aqueous solution using microporous titanosilicate ETS-4. Chem Eng J 147(2–3):173–179

Graham EE, Dranoff JS (1982a) Application of the Stefan–Maxwell equations to diffusion in ion-exchangers. 1. Theory. Ind Eng Chem Fundam 21(4):360–365

Graham EE, Dranoff JS (1982b) Application of the Stefan–Maxwell equations to diffusion in ion-exchangers. 2. Experimental results. Ind Eng Chem Fundam 21(4):365–369

Helfferich F (1995) Ion exchange. Dover, New York

Hogendoorn JA, AJVd Veen, JHGVd Stegen, Kuipers JAM, Versteeg GF (2001) Application of the Maxwell–Stefan theory to the membrane electrolysis process: model development and simulation. Comput Chem Eng 25:1251–1265

Jackson R (1977) Transport in porous catalysts. Elsevier, Amsterdam

Kraaijeveld G, Sumberova V, Kuindersma S, Wesselingh H (1995) Modeling electrodialysis using the Maxwell–Stefan description. Chem Eng J Biochem Eng J 57(2):163–176

Krishna R, Wesselingh JA (1997) Review article number 50—the Maxwell–Stefan approach to mass transfer. Chem Eng Sci 52(6):861–911

Kulov NN, Nikolaishvili EK, Barabash VM, Braginski LN, Malyusov VA, Zhavoronkov NM (1983) Dissolution of solid particles suspended in agitated vessels. Chem Eng Commun 21(4–6):259–271

Lito PF, Silva CM (2008) Comparison between Maxwell–Stefan and Nernst–Planck equations to describe ion exchange in microporous materials. Defect Diffus Forum 273–276:776–781

Lito PF, Cardoso SP, Loureiro JM, Silva CM (2012). Ion-exchange equlibria and kinetics. In: Inamuddin S, Luqman M (eds) Ion-exchange technology: theory, materials and applications, chap 3, pp 51–120. Springer, Berlin

Lopes CB, Otero M, Coinbra J, Pereira E, Rocha J, Lin Z, Duarte A (2007) Removal of low concentration Hg^{2+} from natural waters by microporous and layered titanosilicates. Micropor Mesopor Mat 103(1–3):325–332

Lopes CB, Otero M, Lin Z, Silva CM, Rocha J, Pereira E, Duarte AC (2009) Removal of Hg^{2+} ions from aqueous solution by ETS-4 microporous titanosilicate - Kinetic and equilibrium studies. Chem Eng J 151(1–3):247–254

Lito PF, Aniceto JPS, Silva CM (2013) Modelling ion exchange kinetics in zeolyte-type materials using Maxwell–Stefan approach. Desalination Water Treat. doi:10.1080/19443994.2013.815682

Lv L, Wang K, Zhao XS (2007) Effect of operating conditions on the removal of Pb^{2+} by microporous titanosilicate ETS-10 in a fixed-bed column. J Colloid Interface Sci 305(2):218–225

Miller SA, Amber CM, Bennet RC, Dahlstrom DA, Darji JD, Emmet RC, Gray JB, Gurnham CF, Jacobs LJ, Klepper RP, Michalson AW, Oldshue JY, Silverblatt CE, Smith JC, Todd DB (1984) Liquid–solid systems. In: Perry RH, Green D (eds) Perry's chemical engineers' handbook. McGrow-Hill, Singapore

Misic DM, Sudo Y, Suzuki M, Kawazoe K (1982) Liquid-to-particle mass-transfer in a stirred batch adsorption tank with non-linear isotherm. J Chem Eng Jpn 15(1):67–70

Økland TE, Wilhelmsen E, Solevåg Ø (2005) A study of the priority substances of the Water Framework Directive, monitoring and need for screening. Bergfald & Co., Norway

Otero M, Lopes CB, Coimbra J, Ferreira TR, Silva CM, Lin Z, Rocha J, Pereira E, Duarte AC (2009) Priority pollutants (Hg^{2+} and Cd^{2+}) removal from water by ETS-4 titanosilicate. Desalination 249(2):742–747

Patzay G (1995) A simplified numerical solution method for the Nernst–Planck multicomponent ion exchange kinetics model. React Funct Polym 27(1):83–89

Pinto NG, Graham EE (1987) Characterization of ionic diffusivities in ion-exchange resins. Ind Eng Chem Res 26(11):2331–2336

Rodriguez JF, Valverde JL, Rodrigues AE (1998) Measurements of effective self-diffusion coefficients in a gel-type cation exchanger by the zero-length-column method. Ind Eng Chem Res 37(5):2020–2028

Rodriguez JF, de Lucas A, Leal JR, Valverde JL (2002) Determination of intraparticle diffusivities of Na^{+}/K^{+} in water and water/alcohol mixed solvents on a strong acid cation exchanger. Ind Eng Chem Res 41(12):3019–3027

Samson E, Marchand J (1999) Numerical solution of the extended Nernst–Planck model. J Colloid Interface Sci 215(1):1–8

Schiesser WE (1991) The numerical method of lines. Academic Press, USA

Siegel FR (2002) Environmental geochemistry of potentially toxic metals. Springer, Berlim

Silva CM, Lito PF (2007) Application of the Maxwell–Stefan approach to ion exchange in microporous materials. Batch process modelling. Chem Eng Sci 62(23):6939–6946

Slater MJ (1991) Principles of ion exchange technology. Butterworth-Heinemann, Great Britain

Smith TG, Dranoff JS (1964) Film diffusion-controlled kinetics in binary ion exchange. Ind Eng Chem Fundam 3(3):195–200

Treybal RE (1981) Mass-transfer operations. McGraw-Hill International Editions, Singapore

Valverde JL, De Lucas A, Carmona M, Gonzalez M, Rodriguez JF (2004) A generalized model for the measurement of effective diffusion coefficients of heterovalent ions in ion exchangers by the zero-length column method. Chem Eng Sci 59(1):71–79

van der Stegen JHG, van der Veen AJ, Weerdenburg H, Hogendoorn JA, Versteeg GF (1999) Application of the Maxwell–Stefan theory to the transport in ion-selective membranes used in the chloralkali electrolysis process. Chem Eng Sci 54(13–14):2501–2511

Varshney KG, Pandith AH (1999) Forward and reverse ion-exchange kinetics for some alkali and alkaline earth metal ions on amorphous zirconium(IV) aluminophosphate. Langmuir 15(22):7422–7425

Varshney KG, Gupta PA, Tayal N (2003) Kinetics of ion exchange of alkaline earth metal ions on, acrylamide cerium(IV) phosphate: a fibrous ion exchanger. Colloids Surf B Biointerfaces 28(1):11–16

Wesselingh JA, Vonk P, Kraaijeveld G (1995) Exploring the Maxwell–Stefan description of ion-exchange. Chem Eng J Biochem Eng J 57(2):75–89